

An MRAS Sensorless Technique Based on the MCA EXIN + Neuron for High Performance Induction Motor Drives

UDK 621.313.333.07
IFAC 2.1.4;4.7.1

Original scientific paper

This paper proposes a new sensorless technique for induction motor drives based on a hybrid MRAS-neural technique, which improves a previously developed neural MRAS based sensorless method. In this paper the open-loop integration in the reference model is performed by an adaptive neural integrator, enhanced here by means of a speed-varying filter transfer function. The adaptive model is based on a more accurate discrete current model based on the modified Euler integration, with a resulting more stable behaviour in the field weakening region. The adaptive model is further trained on-line by a generalized least squares technique, the MCA EXIN + neuron, in which a parameterized learning algorithm is used. As a consequence, the speed estimation presents an improved convergence with higher accuracy and shorter settling time, because of the better transient behaviour of the neuron.

A test bench has been set up to verify the methodology experimentally and the results prove its goodness at very low speeds (below 4 rad/s) and in zero-speed operation.

Key words: induction motor drives, sensorless control, model reference adaptive systems, neural networks

1 INTRODUCTION

This work deals with sensorless control of induction motor drives [1-10] and in particular with the rotor speed estimation by means of MRAS observers [11-15]. Specifically, this work is in the framework of series of papers dealing with sensorless control in AC drives, based on the fundamental mmf dynamic model of the induction machines in which the speed computation is obtained by means of least squares techniques [16-20]. In particular, the dynamical performances and the estimation accuracy were previously shown with a Total Least-Squares (TLS) method, while now this paper presents an improved MRAS observer for three aspects: firstly, a more accurate discrete current model is used, based on the modified Euler integration (see [19] for all the details about the advantages of the proposed modified Euler integration method), secondly in the reference model an enhanced version of the adaptive integration technique of [17, 20, 21] has been used with a filter whose transfer function varies with speed, and thirdly a completely new neural technique, the MCA EXIN + neuron, has been adopted to estimate the rotor speed. Each of these improvements has respectively given the following advantages: more stable flux estimation, more accurate open loop flux integration at very low speed than the fixed-pole filter transfer function

and finally the use of the MCA EXIN + neuron with its scheduling makes it more powerful than the other existing techniques with resulting smoother transient, shorter settling time and better accuracy [24]. The use of the MCA EXIN + neuron makes allowances for the measurement flux modeling errors, which influence the accuracy of the speed estimation, since MCA EXIN+ is inherently robust to the two above sources of errors. The MCA EXIN+MRAS observer has been experimentally tested on a rotor-flux-oriented vector control drive with an induction motor.

2 LIMITS OF MODEL BASED SENSORLESS TECHNIQUES

A. Open-loop integration

One of the main problems of some speed observers, when adopted in high performance drives, is the open-loop integration in presence of DC biases. Speed observers suffering from this problem are those which employ open-loop flux estimators, e.g. open-loop speed estimators and those MRAS systems where the reference model is an open-loop flux estimator [11, 13-15]. Unlike them, speed estimators employing such closed-loop flux integration as the classic full-order Adaptive Observer [3], do not have this problem.

In particular this problem is due to DC drifts, which are always present in the signal both before it is integrated, thus causing the integrator to saturate with a resulting inadmissible estimation error, and after the integration, because of the initial conditions. In general Low Pass (LP) filters with very low cut-off frequency are used instead of pure integrators [13–15]; however since they fail in low frequency ranges, close to their cut-off frequency, some alternative solutions have been devised to overcome this problem, e.g. the integrator with saturation feed-back [25], the integrator based on cascaded LP filters [26, 27], the integrator based on the off-set vector estimation and compensation of residual estimation error [28] and the adaptive neural integrator [21]. In this work, the adaptive neural integrator proposed in [21] has been adopted and further improved by means of a filter whose transfer function varies with speed, as fully explained in § 3 B.

B. Inverter non-linearity

The power devices of an inverter present a finite voltage drop in »on-state«, due to their forward non-linear characteristics. This voltage drop has to be taken into consideration at low frequency (low voltage amplitude) where it becomes comparable with the stator voltage itself, giving rise to distortion and discontinuities in the voltage waveform. Here the compensation method proposed by [29] has been employed. This technique is based on modelling the forward characteristics of each power device by a piecewise linear characteristic, with an average threshold voltage and an average differential resistance.

C. Machine Parameter Mismatch

A further source of error in flux estimation is the mismatch of the stator and rotor resistances of the observer with their real values because of heating/cooling of the machine. The load dependent variations of the winding temperature may lead up to 50 % error in the modelled resistance. Stator and rotor resistances should be therefore estimated on-line and tracked during the operation of the drive. A great deal of on-line parameter estimation algorithms have been devised [1, 3, 28–31], requiring low complexity and computational burden when used in control systems. In any case, it should be emphasized that steady-state estimation of the rotor resistance cannot be performed in sensorless drives, thus rotor resistance variations must be deduced from stator resistance estimation. In the case under study, the stator estimation methodology proposed in [28], employed also in [17], has been adopted.

3 THE TLS MRAS OBSERVER

A. Structure of the Observer

In the MRAS speed observation scheme proposed here the reference model is based on the well known voltage model of the induction motor [1], while the adaptive model is a linear artificial neural network based on the current model. To perform open-loop integration the voltage model employs the adaptive neural integrator based on the neural adaptive filtering described in § 3 B.

The adaptive model is given by:

$$\begin{cases} T_r \frac{d\psi_{rd}}{dt} = L_m i_{sD} - \psi_{rd} - \omega_r T_r \psi_{rq} \\ T_r \frac{d\psi_{rq}}{dt} = L_m i_{sQ} - \psi_{rq} + \omega_r T_r \psi_{rd} \end{cases} \quad (1)$$

Eq (1) can be re-written in the following manner:

$$\dot{\Psi}_r' = \mathbf{A}_x \Psi_r' + B_x \mathbf{i}_s \quad (2)$$

where

$$\Psi_r' = \begin{bmatrix} \psi_{rd} \\ \psi_{rq} \end{bmatrix}, \quad \mathbf{A}_x = \begin{bmatrix} -1 & -\omega_r T_r \\ \omega_r T_r & -1 \end{bmatrix}, \quad B_x = L_m \mathbf{i}_s = \begin{bmatrix} i_{sD} \\ i_{sQ} \end{bmatrix}.$$

Its corresponding discrete model is given by:

$$\hat{\Psi}_r'(k) = e^{\mathbf{A}_x T_s} \hat{\Psi}_r'(k-1) + [e^{\mathbf{A}_x T_s} - \mathbf{I}] \mathbf{A}_x^{-1} B_x \mathbf{i}_s(k-1) \quad (3)$$

where k is the current sampling time.

$e^{\mathbf{A}_x T_s}$ is generally computed by truncating its power series expansion at the n -th term, i.e.

$$e^{\mathbf{A}_x T_s} = \mathbf{I} + \frac{\mathbf{A}_x T_s}{1!} + \frac{\mathbf{A}_x^2 T_s^2}{2!} + \dots + \frac{\mathbf{A}_x^n T_s^n}{n!} \quad (4)$$

In the MRAS observer proposed here, the adaptive model is based on an enhanced ADALINE neural network based on a modified Euler discretization method, which is capable of solving the instability problems due to the simple Euler discretization process. Moreover, like [17], the adaptive model has been employed in »prediction mode«, that is the flux components computed with the reference model are used in the adaptive model, thus avoiding any feedback.

The employment of the adaptive model in prediction mode leads to a quicker convergence of the algorithm, a higher bandwidth of the speed control loop, a better behaviour at zero speed, lower speed estimation errors both in transient and steady-state conditions and a far more stable behaviour of the estimator, in particular in the field-weakening region, as explained in § 4.

A more efficient integration method than that used in [17], that is the Modified Euler Integration, has been employed in (3) and it takes into consideration also the values of the variables in two previous time steps [22]. The following discrete time equations are obtained:

$$\begin{aligned}\hat{\psi}_{rd}(k) &= w_{1n} \hat{\psi}_{rd}(k-1) - w_{2n} \hat{\psi}_{rq}(k-1) + w_{3n} i_{sD}(k-1) + \\ &\quad + w_{4n} \hat{\psi}_{rd}(k-2) + w_{5n} \hat{\psi}_{rq}(k-2) - w_{6n} i_{sD}(k-2) \\ \hat{\psi}_{rq}(k) &= w_{1n} \hat{\psi}_{rq}(k-1) + w_{2n} \hat{\psi}_{rd}(k-1) + w_{3n} i_{sQ}(k-1) + \\ &\quad + w_{4n} \hat{\psi}_{rq}(k-2) - w_{5n} \hat{\psi}_{rd}(k-2) - w_{6n} i_{sQ}(k-2)\end{aligned}\quad (5)$$

where $\hat{}$ marks the variables estimated with the adaptive model and k is the current time sample. A linear neural network can reproduce these equations, where $w_{1n}, w_{2n}, w_{3n}, w_{4n}, w_{5n}, w_{6n}$ are the weights of the neural networks defined as: $w_{1n} = 1 - 3T_s/(2T_r)$, $w_{2n} = 3\omega_r T_s/2$, $w_{3n} = 3T_s L_m/(2T_r)$, $w_{4n} = T_s/(2T_r)$, $w_{5n} = \omega_r T_s/2$, $w_{6n} = T_s L_m/(2T_r)$.

Rearranging (5), the following matrix equation is obtained in prediction mode:

$$\begin{aligned}&\begin{bmatrix} -3/2 T_s \psi_{rq}(k-1) + 1/2 T_s \psi_{rq}(k-2) \\ 3/2 T_s \psi_{rd}(k-1) - 1/2 T_s \psi_{rd}(k-2) \end{bmatrix} \omega_r(k-1) = \\ &= \begin{bmatrix} \hat{\psi}_{rd}(k) - w_{1n} \psi_{rd}(k-1) - w_{3n} i_{sD}(k-1) - w_{4n} \psi_{rd}(k-2) + w_{6n} i_{sD}(k-2) \\ \hat{\psi}_{rq}(k) - w_{1n} \psi_{rq}(k-1) - w_{3n} i_{sQ}(k-1) - w_{4n} \psi_{rq}(k-2) + w_{6n} i_{sQ}(k-2) \end{bmatrix}.\end{aligned}\quad (6)$$

This matrix equation can be solved by any regression technique. Here the MCA EXIN+ technique has been adopted to retrieve the rotor speed on-line. Figure 1 shows the block diagram of the corresponding MRAS speed observer.

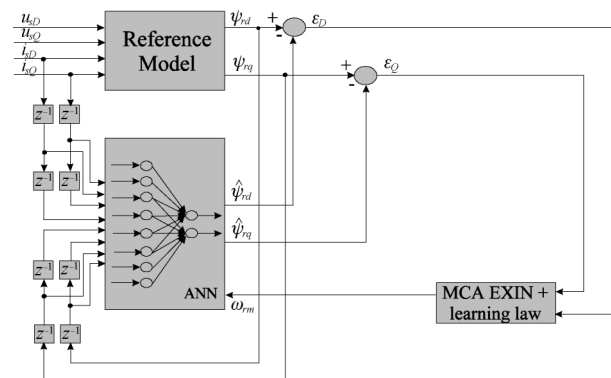


Fig. 1 Block diagram of the ANN MRAS observer with modified Euler adaptive model (adaptive model in prediction mode)

B. The Adaptive Integrator based on Neural Filterin

The neural adaptive integrator proposed in [21] and adopted in the TLS MRAS observer both in a FOC (Field Oriented Control) [17] and DTC (Di-

rect Torque Control) [20] drive, has been here improved in its low frequency behaviour by making its learning factor τ adaptive, according to the reference speed of the machine. The idea is to use linear filter (ADALINE) used as a notch filter to cut off the DC component adaptively.

The learning law of the neural adaptive filter is as follows:

$$y(k+1) = y(k) + 2\tau(d(k) - y(k)) \quad (7)$$

where k is the current time instant, $d(k)$ is the primary input of the filter, $y(k)$ is the output of the filter neuron and τ is the learning rate. This one-weight neuron is able to remove not only a constant bias but also a slowly varying drift in the primary input. It should be remarked that two neural filters must be used in the neural-based integrator: the neural filter 1 eliminates the DC component of the signal to be processed, the neural filter 2 eliminates the DC drift appearing at the output of the integrator because of the initial conditions and the filtering error of the neural filter 1 during its adaptation (Figure 2), as shown below.

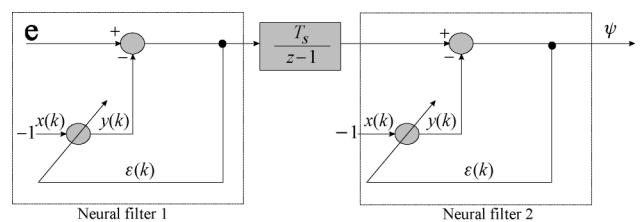


Fig. 2 Neural filter based integrator

Figure 3 shows the frequency response of an ideal integrator, an LP filter based integrator (cut-off frequency = 15 rad/s) and the neural adaptive integrator with two different values of τ , respectively $2 \cdot 10^{-4}$ and $1 \cdot 10^{-5}$. It can be demonstrated that the transfer function of the neural adaptive integrator presents two poles and one zero (in the origin). This figure shows that the adaptive neural integrator with $\tau = 2 \cdot 10^{-4}$ outperforms the LP filter, both in its magnitude and phase characteristics, in the neighbourhood of a reference speed of about 10 rad/s in electrical angles (corresponding to 5 rad/s in mechanical ones). However, if a speed below 5 rad/s is required, a neural integrator with $\tau = 1 \cdot 10^{-5}$ offers a better behaviour, since it approximates the ideal integrator well at much lower frequencies. Nevertheless, a neural integrator with $\tau = 1 \cdot 10^{-5}$ can-

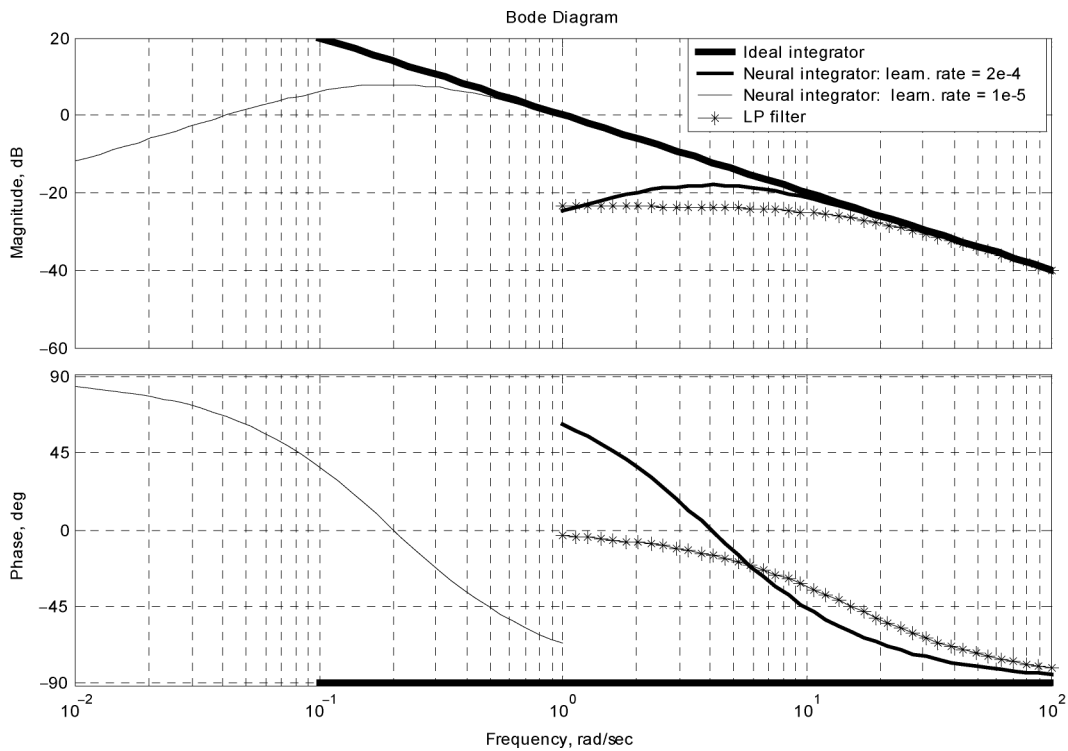


Fig. 3 Frequency response of the adaptive integrator with two values of the learning factor, of the LP integrator and of the ideal integrator

not be suitably employed in the whole speed range of the drive, since the adaptation time of the filter increases when the value of τ decreases, as shown in Figure 4, which shows the difference between the adaptation times obtained with the two values of τ at the operating speed of 2 rad/s, when a 2 % (of the rated voltage) dc signal is superimposed to the voltage signal on phase sA. This figure clearly shows that a lower value of τ permits a better flux estimation, but at the expense of a high filtering adaptation time. For this reason, the use of low

values of τ can bring about stability problems in the flux control loop, especially when a speed transient is required. In this respect the problem has been solved as follows: at reference speeds above 10 rad/s (in electrical angles) and during each speed transient the value of τ has been set to $2 \cdot 10^{-4}$, while in speed steady-state at references from 10 down to 4 rad/s, the value of τ has been varied linearly from $2 \cdot 10^{-4}$ to $1 \cdot 10^{-5}$ and then kept to this last value for lower reference speeds, as shown in Figure 5. It should be remarked that reducing the value of τ corresponds to moving the poles of the neural filter towards the origin, which however does not affect anyhow the accuracy of the integrator. This is not the case for the LP filter integrator, where the amplitude of the pole cannot be reduced too much, since the lower the amplitude of the pole the higher the drift at the LP filter output caused by a DC drift at its input.

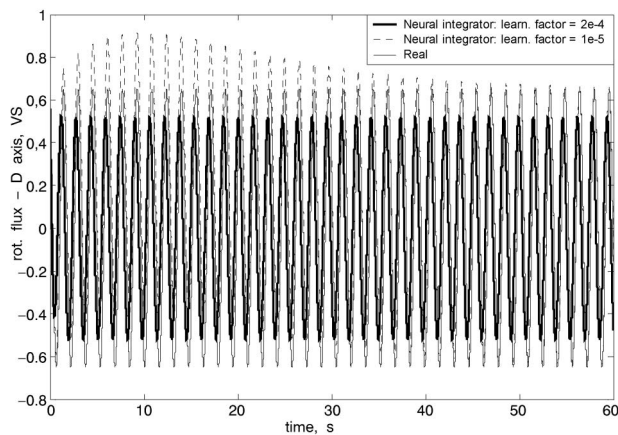


Fig. 4 Rotor flux D axis component obtained with a 2 % (of the rated voltage) dc signal superimposed to the voltage signal on phase sA, with two values of τ (simulation)

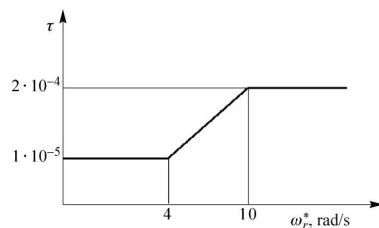


Fig. 5 Variation of the learning factor according to the reference speed of the machine

4 STABILITY ISSUES IN FIELD WEAKENING WITH SIMPLE EULER AND MODIFIED EULER INTEGRATION

This section is a description of the stability considerations explained in [19] and is rewritten shortly here for clarity reasons.

Some considerations fully justify the use of the adaptive model in prediction mode with the modified Euler integration. When used in simulation mode, the process output, that is the rotor flux linkage, is delayed and then used as an input. In case the simple Euler integration method were used, then the transfer function $X(z)$ of the flux model in the z -domain is:

$$X(z) = \frac{Z(\hat{\Psi}'_r(k))}{Z(\hat{i}_s(k-1))} = \frac{w_3}{(jw_2 + w_1)z^{-1} - 1} = \frac{w_3 z}{(jw_2 + w_1) - z} \quad (8)$$

which has one pole $z_1 = w_1 + jw_2$, and one zero at the origin of the z -domain. For stability reasons, the poles of the transfer function must lie within the unit circle in the z -domain. There is therefore a critical value of the rotor speed which causes instability of the system. More precisely, the following relationships must be satisfied:

$$-\frac{1}{T_s} \sqrt{\frac{T_s}{T_r} \left(2 - \left(\frac{T_s}{T_r} \right) \right)} < \omega_r < \frac{1}{T_s} \sqrt{\frac{T_s}{T_r} \left(2 - \left(\frac{T_s}{T_r} \right) \right)} \quad (9)$$

and

$$T_s < \frac{2T_r}{1 + T_r^2 \omega_r^2}. \quad (10)$$

Relationship (9) shows that the drive goes into instability for increasing values of the rotor speed, while relationship (10) shows that there is the an upper limit of stability of sampling time T_s , if the motor runs at a defined angular speed.

For instance, for the motor at hand whose rated speed is 314 electrical rad/s and $T_r = 0.134$ s, this upper limit for the sampling time is of 0.15 ms. Conversely, if a sampling time of 0.1 ms is employed, which is the case under study, the highest limit of the speed is of 385 electrical rad/s (Figure 6, upper graph), which implies that the speed can be increased to as much as 18 % of the rated speed and not over this limit, with resulting difficulties in using the drive in the field-weakening region.

To overcome this difficulty the adaptive model should be used in prediction mode, that is the delayed outputs of the reference model are used as inputs to the adaptive model. In this case no feedback exists and no stability problems occur.

The simple Euler method was obtained by using $n=1$ in (4). Better stability results, can be obtained if $n=2$ is chosen in (4). Then the speed stability limit increases as shown in Figure 6, bottom graph. This approximation has been at least used in [13–15] to avoid the stability problems in simulation mode. It should be emphasized that this last method implies at least the on-line computation of the square of the $A_x T_s$ matrix, which makes this method too cumbersome for on-line applications.

Better results, at the expense of a slight increase of computation in comparison with the simple Euler method, can be obtained with the modified Euler method [19, 22]. In this case a similar analysis of stability shows that two poles of the transfer

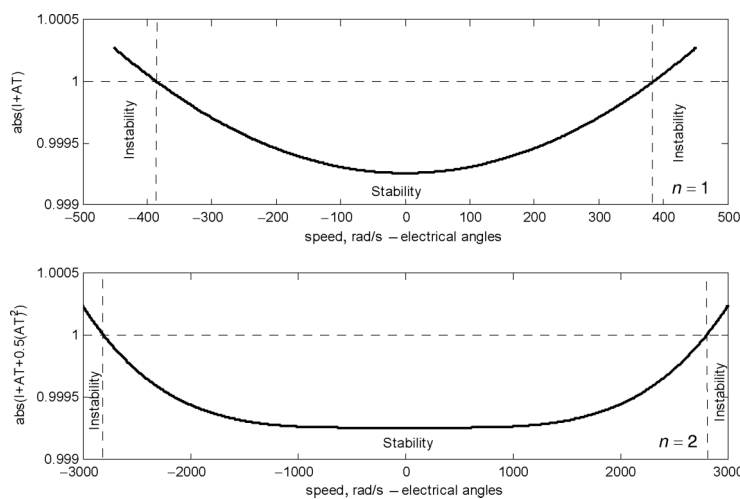


Fig. 6 Amplitude of the poles in simple Euler integration with the approximated exponential function with $n=1$ and $n=2$

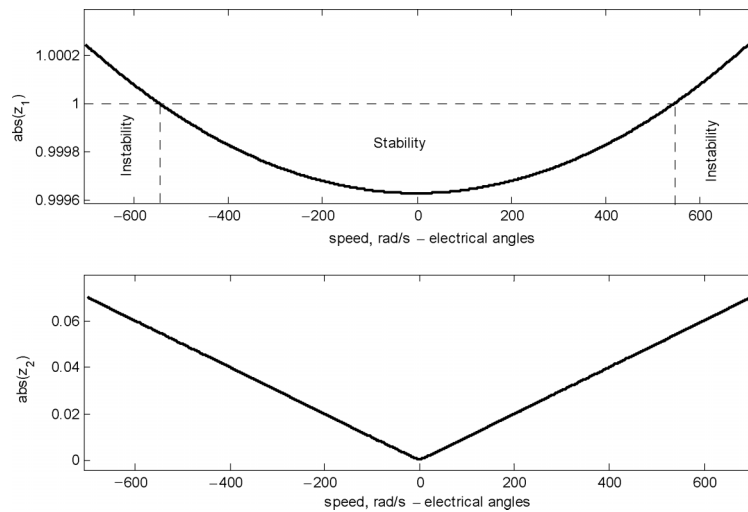


Fig. 7 Amplitude of the poles with the modified Euler integration

function vary with speed, but the resulting speed stability limit is much higher than that obtained with the simple Euler method, thus allowing the exploitation of the field weakening region (Figure 7).

5 THE MCA EXIN + NEURON IN SENSORLESS CONTROL

A. Least-Squares Techniques

Matrix equation (6), which can be written more generally as $\mathbf{Ax} \approx \mathbf{b}$, can be solved for ω_r by using Least-Squares (LS) techniques. In particular in literature there exist three Least-Squares techniques, i.e. the Ordinary Least-Squares (OLS), the Total Least-Squares (TLS) and the Data Least-Squares (DLS) which arise when errors are respectively present only in \mathbf{b} or both in \mathbf{A} and in \mathbf{b} or only in \mathbf{A} .

In classical Ordinary Least-Squares (OLS) each element of \mathbf{A} is considered without any error: therefore all errors are confined to \mathbf{b} . However this hypothesis does not always correspond to the reality: modelling errors, measurement errors etc. can in fact cause errors also in \mathbf{A} . Therefore in real world applications the employment of Total Least-Squares would be very often better, as it takes into consideration also the errors in the data matrix.

In the mono-dimensional case ($n = 1$), which is the case under study, the resolution of the LS problem consists in determining the angular coefficient ω_r of the straight line of equation $\mathbf{A}\omega_r \approx \mathbf{b}$. The LS technique solves for this problem by calculating the value of ω_r which minimises the sum of squares of the distances among the elements (a_i, b_i) , with $i = 1, \dots, m$, and the line itself. Figure 8 shows the difference among the OLS, TLS and DLS. OLS minimises the sum of squares of the distances in the \mathbf{b} direction (error only in the obser-

vation vector). TLS minimises the sum of squares in the direction orthogonal to the line (for this reason TLS is also called orthogonal regression) while DLS minimises the sum of squares in the \mathbf{A} direction (errors only in the data matrix). In particular it must be expected that, in absence of noise, the results obtained with TLS are equal to those obtained with OLS; however in presence of increasing noise the performance of TLS remains higher than that of OLS, as TLS is less sensitive to noise. For these reasons the TLS algorithm is particularly suitable for estimation processes in which data are affected by noise or modelling errors; this is certainly the case of speed estimation, where the estimated rotor flux, present in \mathbf{A} , is affected both by modelling errors and noise. Therefore, a TLS technique should be used instead of the Ordinary Least-Squares (OLS) technique. The TLS EXIN neuron, which is the only neural network capable to solve a TLS problems recursively on-line, has been successfully adopted in MRAS speed observers [17, 20]. In this work, a new generalized Least-Squares technique, the MCA EXIN+ (Minor Component Analysis) neuron, is used for the first time to compute the rotor speed. This technique is a further improvement of the TLS EXIN neuron [23, 24] and is explained below.

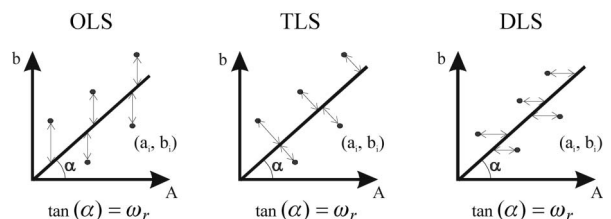


Fig. 8 Schematics of the Least-Squares techniques in the mono-dimensional case

B. The MCA EXIN + neuron

As written above, eq. (6) can be solved by using different techniques according to the assumptions about noise in the data; indeed, if only the observation vector \mathbf{b} is corrupted by noise, the problem is ordinary least squares (OLS), if only the data matrix is corrupted by noise, the problem is data least squares (DLS), if all data are corrupted by noise, as the problem considered in this work, the problem is TLS, due to measurement and flux modelling errors. In [23] all these problems have been generalized by using a parameterized formulation (Generalized TLS, GeTLS EXIN) of an error function whose minimization yields the corresponding solution. This error is given by:

$$E(\mathbf{x}) = \frac{(\mathbf{A}\mathbf{x} - \mathbf{b})^T (\mathbf{A}\mathbf{x} - \mathbf{b})}{1 - \zeta + \zeta \mathbf{x}^T \mathbf{x}} \quad (11)$$

where T represents the transpose and ζ is equal to 0 for OLS, 0.5 for TLS and 1 for DLS. The corresponding iterative algorithm (GeTLS EXIN learning law), which computes the minimizer by using an exact gradient technique, is given by:

$$\mathbf{x}(k+1) = \mathbf{x}(k) - \alpha(k)\gamma(k)\mathbf{a}(k) + \left[\zeta\alpha(k)\gamma^2(k)\mathbf{x}(k) \right] \quad (12)$$

where:

$$\gamma(k) = \frac{\mathbf{a}(k)^T \mathbf{x}(k) - \mathbf{b}(k)}{1 - \zeta + \zeta \mathbf{x}(k)^T \mathbf{x}(k)} \quad (13)$$

being $\alpha(k)$ the learning rate, $\mathbf{a}(k)$ the row of \mathbf{A} fed at instant k and $\mathbf{b}(k)$ the corresponding observation. The GeTLS EXIN learning law becomes the TLS EXIN learning law for ζ equal to 0.5 [23]. The TLS EXIN problem can also be solved by scheduling the value of the parameter in GeTLS EXIN, e.g. it can vary linearly from 0 to 0.5 and then remains constant. This scheduling improves the transient, the speed and the accuracy of the iterative technique. [24] shows that a TLS problem corresponds to a minor component analysis (MCA) problem and is equivalent to a particular DLS problem. Indeed, define $\mathbf{C} = [\mathbf{A}; \mathbf{b}]$ as the augmented matrix built by appending the observation vector to the right of the data matrix. In this case the linear regression problem can be reformulated as $\mathbf{C} \begin{bmatrix} \mathbf{x} \\ -1 \end{bmatrix} \approx \mathbf{0}$ and can be solved as a homogeneous system $\mathbf{C}\mathbf{v} \approx \mathbf{0}$; the solution \mathbf{v} is given by the eigen vector associated to the smallest eigenvalue of $\mathbf{C}^T\mathbf{C}$ (MCA). This eigenvector can be found by minimizing the following error function:

$$E(\mathbf{v}) = \frac{\mathbf{v}^T \mathbf{C}^T \mathbf{C} \mathbf{v}}{\mathbf{v}^T \mathbf{v}} \quad (14)$$

which is the Rayleigh quotient of $\mathbf{C}^T\mathbf{C}$. Hence, the TLS solution \mathbf{x} is found by normalizing \mathbf{v} in order to have the last component equal to -1 . Resuming, TLS can be solved by applying MCA to the augmented matrix \mathbf{C} . In [24] it is also proved the equivalence between MCA and DLS in a very specific case. Indeed, setting $\mathbf{b} = \mathbf{0}$ and $\zeta = 1$ (DLS) in eq. (11) yields eq. (14) with $\mathbf{C} = \mathbf{A}$. Hence, the MCA for the matrix \mathbf{C} is equivalent to the DLS of the system composed of \mathbf{C} as the data matrix and of a null observation vector. In particular, TLS by using MCA can be solved by using eq.s (12)–(13) with $\mathbf{b} = \mathbf{0}$ and $\zeta = 1$ with $\mathbf{C} = \mathbf{A}$. The advantage of this approach is the possibility of using the scheduling. This technique is the learning law of the MCA EXIN + neuron [24], which is an iterative algorithm from a numerical point of view. It yields better results than the other MCA iterative techniques because of its smoother dynamics, faster convergence and better accuracy, which are the consequence of the fact that the varying parameter drives $\mathbf{x}(t)$ toward the solution in a smooth way. These features allow higher learning rates for accelerating the convergence and smaller initial conditions (in [24] it is proven that very low initial conditions speed up the algorithm).

6 EXPERIMENTAL RESULTS

The MCA EXIN + MRAS speed observer has been verified numerically in simulation and applied experimentally on a properly devised test setup [17, 20]. Simulations have been performed in Matlab®–Simulink®. With regard to the experimental tests the speed observer as well as the whole control algorithm have been implemented by software on the DSP of the dSPACE 1103. In particular the speed observer has been tested in a rotor flux oriented scheme (FOC). The adopted MRAS speed observer has been integrated with the R_s estimation algorithm presented in [28] and with the IGBT voltage drop compensation presented in [29]. In all reported experimental results the following ζ scheduling has been adopted: at each speed transient commanded by the control system, a linear variation of ζ from 0 to 1 in 0.3 s has been given. In this way, the flatness of the OLS error surface around its minimum, which prevents the algorithm from being fast, is smoothly replaced by a ravine in the corresponding DLS error surface, which speeds up the convergence to the solution (minimum of eqn. (11)) as well as its final accuracy. Figure 9 clearly shows the error surfaces obtained with $\zeta = 0$ (OLS) and $\zeta = 1$ (DLS) and the MCA EXIN + error trajectory versus the two components of \mathbf{x} with regard to the DLS error surface, obtained when a speed step reference from 0 to 150 rad/s has been given to the drive.

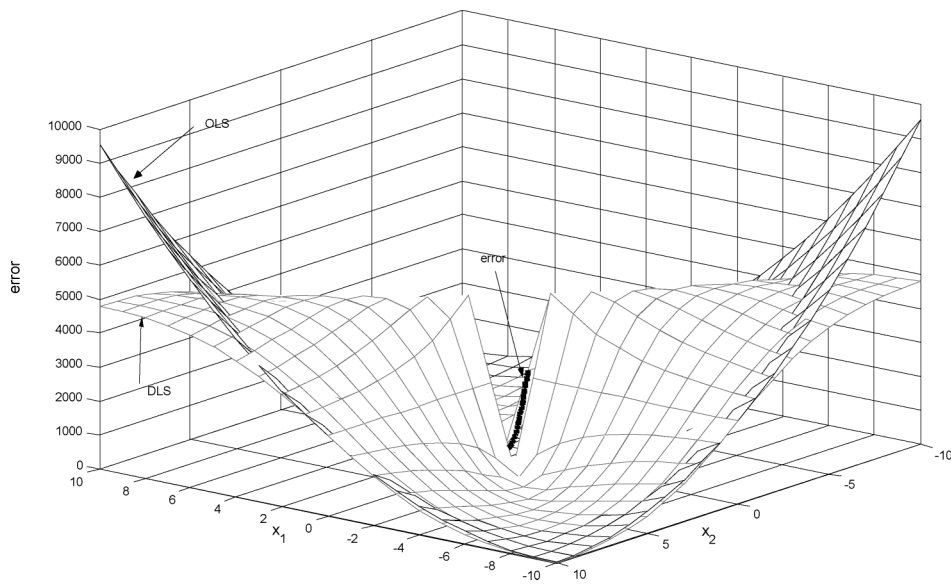


Fig. 9 Error surfaces with $\zeta=0$ and $\zeta=1$ and the MCA EXIN+error trajectory versus x

In the following a series of experimental tests is reported.

A. Stability in Field-Weakening

This test has been performed to verify the stability issues in field weakening of the MCA EXIN + MRAS observer with Modified Euler integration

in comparison with the BPN MRAS observer with Simple Euler integration. As explained above, in fact, this last one suffer from potential instability problems above certain speeds.

The top graph in Figure 10 shows the MCA EXIN + MRAS observer in prediction mode with the modified Euler integration. It shows that no in-

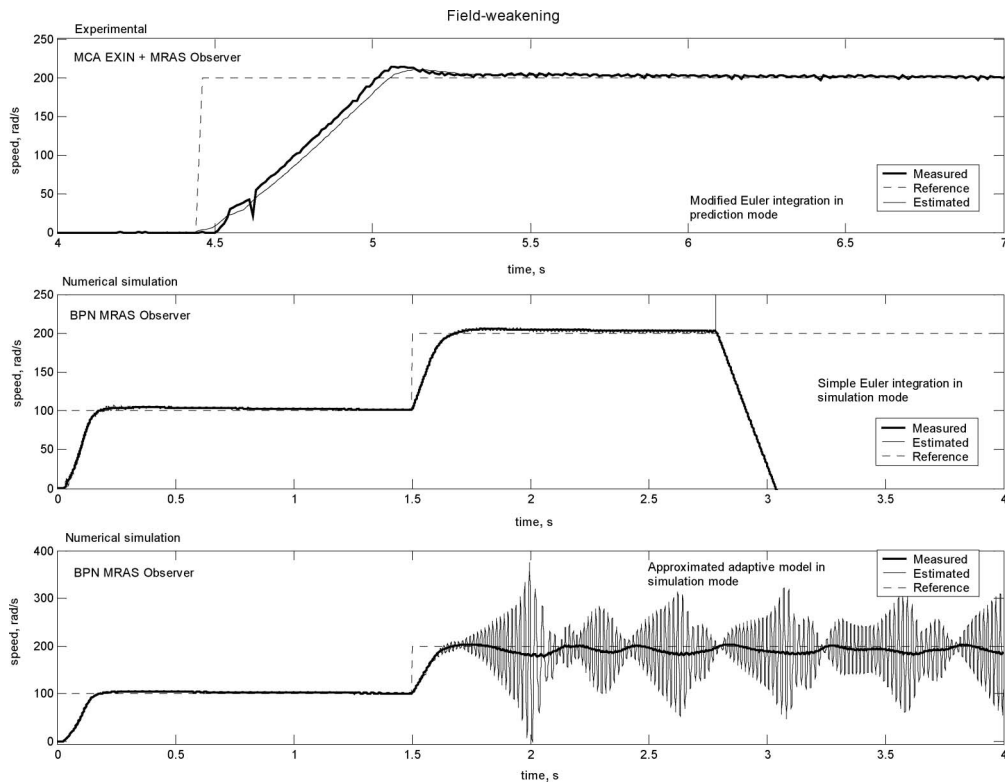


Fig. 10 Reference, measured and estimated speed in field-weakening operation with MRAS observers (experimental and simulation)

stability phenomena occur in field weakening, as expected. In this test the drive has been given a speed reference step of 200 rad/s at no load.

In contrast to this, the BPN MRAS Observer used in simulation mode with both the simple Euler integration and the approximated model [15] shows instability phenomena. As for the BPN MRAS Observer with simple Euler integration, as explained in above, a certain speed stability threshold exists depending on the sampling time. For the motor at hand and a sampling time of 10^{-4} s, this speed threshold is 192 rad/s (mechanical angles). The second graph in Figure 10 shows the reference, the real and the estimated speed when two speed references, respectively of 100 rad/s and 200 rad/s, are given. It shows instability at about 200 rad/s.

As for the BPN MRAS Observer with the approximated adaptive model in simulation mode (this means that $n=2$ has been used in the power expansion (4) as in [13–15]), there exists an increase of the speed threshold which permits the operation in field weakening at the expense though of increased computational burden. However, Figure 10 bottom graph shows that the drive at 200 rad/s

tends to approach to instability with a large estimation error and with huge oscillations of the estimated speed: this is caused by the difficulties in choosing a proper learning factor and momentum in the BPN algorithm. This difficulty in the heuristics of the choice of the parameters does not exist in case a linear neural network were employed. This also implies the use of a low-pass filter of the estimated speed in order to use it in a closed-loop speed control.

B. Dynamic Performances

The dynamic performance of the drive has been tested both at high and low speed. Firstly, a speed reversal from -100 rad/s to 100 rad/s at no load has been given. Figure 11 shows the waveforms of the reference, estimated (used in the feed-back loop) and measured speed as well as the i_{sy} stator current component and the parameter ζ during the test. It shows that both the measured and the estimated speed correctly follow the reference during the speed transient, even when the speed of the drive passes through zero. Secondly, the transient of the observer at lower speeds have been tested. At first, the drive has been given a set of speed rever-

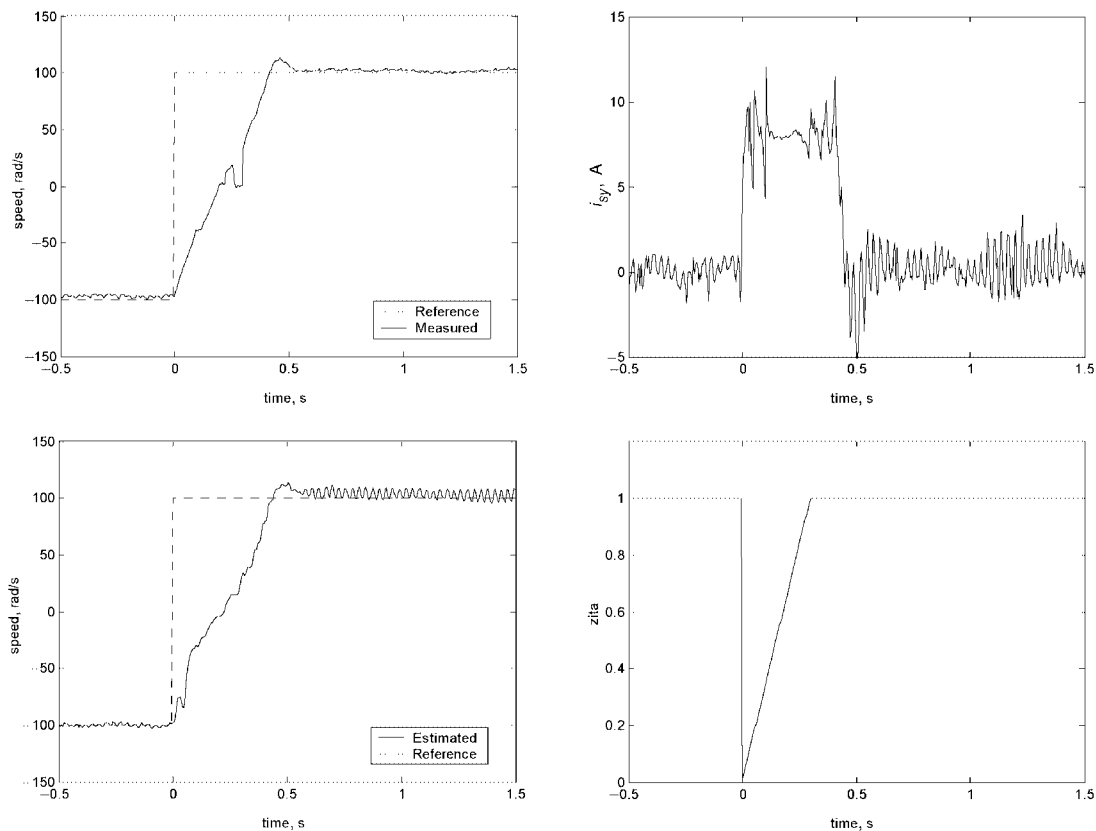


Fig. 11 Reference, estimated and measured speed, i_{sy} and ζ during a -100 to 100 rad/s speed reversal at no load (experimental)

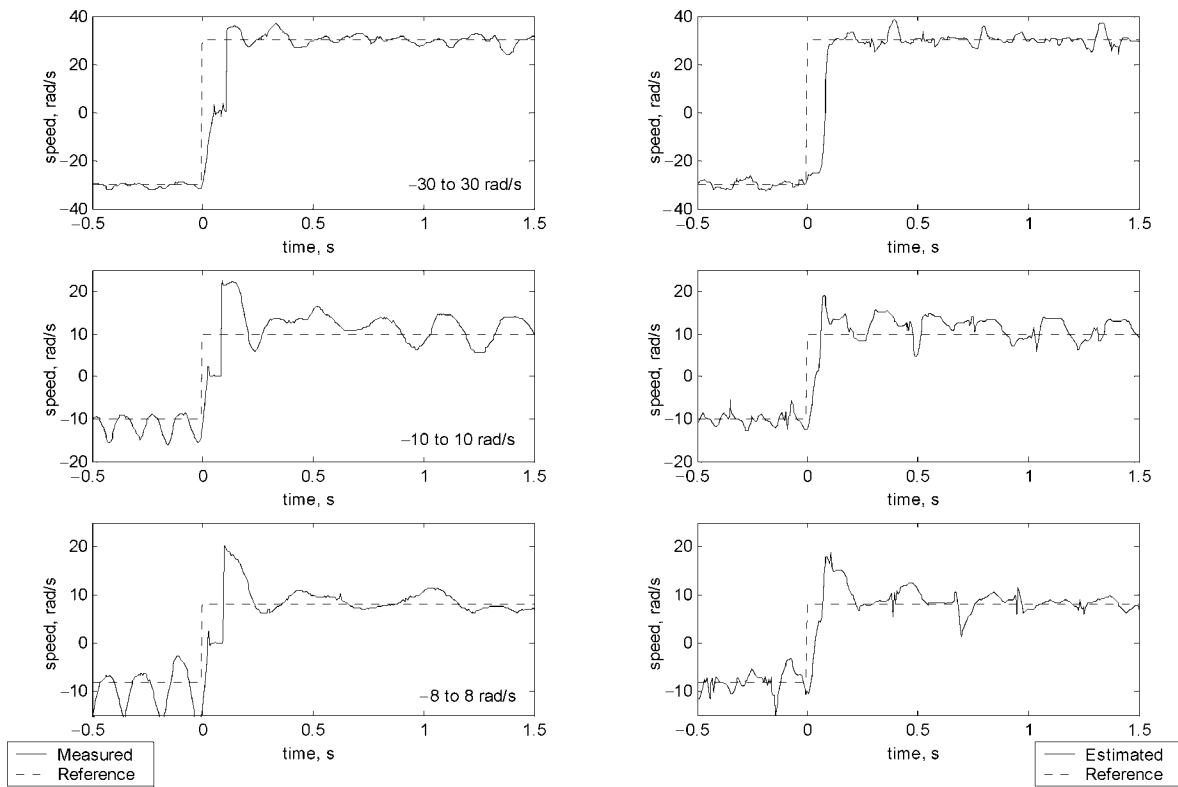


Fig. 12 Reference, estimated and measured speed during a set of speed reversals at no load (experimental)

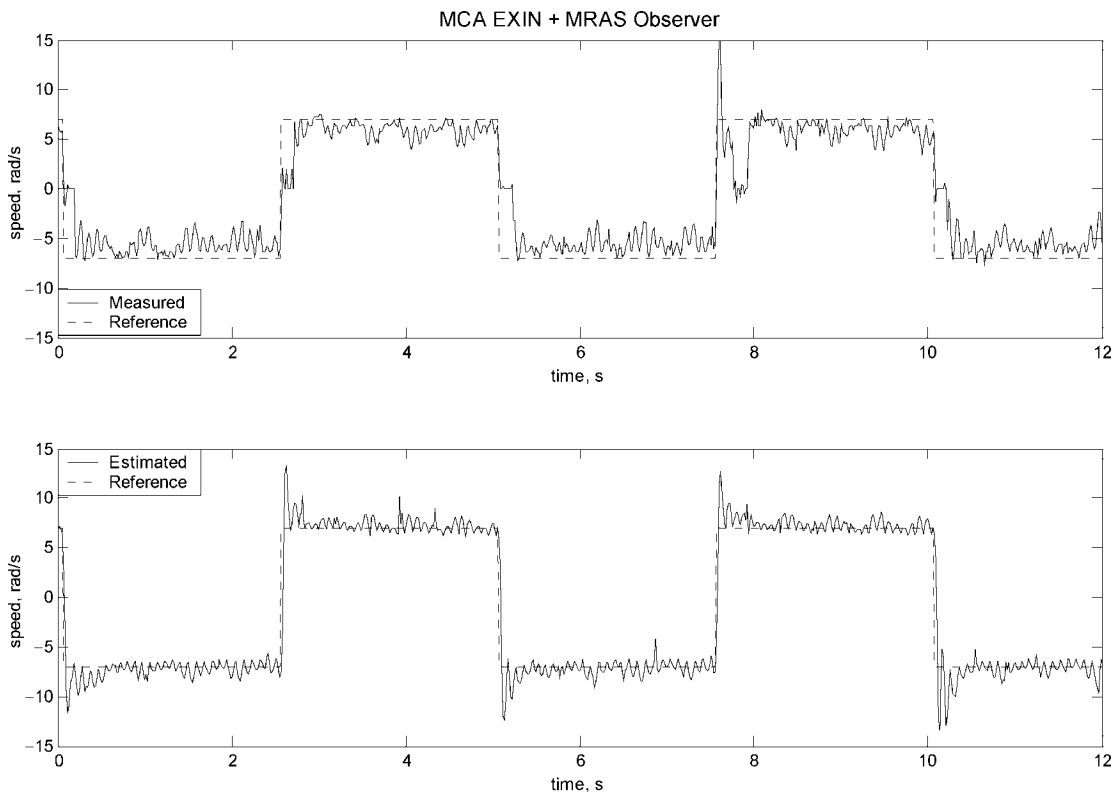


Fig. 13 Reference, measured and estimated speed in a square wave reference of amplitude 7 rad/s and pulsation 0.2 rad/s (experimental)

sals at from -30 to 30 rad/s, from -10 to 10 rad/s and from -8 to 8 rad/s. Figure 12 shows the waveforms of the reference, estimated and measured speed during this test. It clearly highlights a very good dynamic behaviour of the drive, even at low speed. In fact, the challenging speed reversal at low speed is correctly performed by the drive, and the estimated speed correctly follows the real one, without a significant delay time. Thirdly, the dynamic performances of the MCA EXIN + MRAS Observer have been tested by giving the drive a square wave speed reference with the lowest possible amplitude and the highest possible pulsation. Figure 13 shows the reference, measured and estimated speed obtained giving the MCA EXIN + MRAS Observer a square waveform reference of amplitude 7 rad/s and pulsation 0.2 rad/s. These last figures show the capability of this observer to follow a square waveform reference of very low amplitude and highest possible frequency.

C. Low Speed Steady-state operation

To verify the low speed working capability of the drive, it has been operated at the minimum constant speed reference. In this case, the constant very low speed of 3.3 rad/s at no load has been reached.

Figure 14 shows the waveforms of the reference, estimated and measured speed and the estimated stator resistance of the motor during this test. The mean estimation percent error, in this challenging condition, is as low as 18% . Below this speed the machine remains at standstill (zero speed), even if the estimated speed follows correctly its reference, and therefore the observer has not a reliable behaviour. It should be remarked that minimum working speed is lower than that reached both in [17] and [20], thanks to the improved features of the MRAS observer.

D. Zero-Speed operation

Finally, to test the operating capability of the observer at zero speed, the drive has been made to work for 50 s fully magnetized at zero speed with no load. Figure 15, which shows the reference, estimated, and measured speed during this test, clearly highlights the zero speed capability of this observer. In fact, the estimated speed has slight oscillations around 0 rad/s while the measured speed is always zero, except for some spikes which are due to the non-perfect filtering of the speed signal coming from the incremental encoder: in any case the rotor does not move.

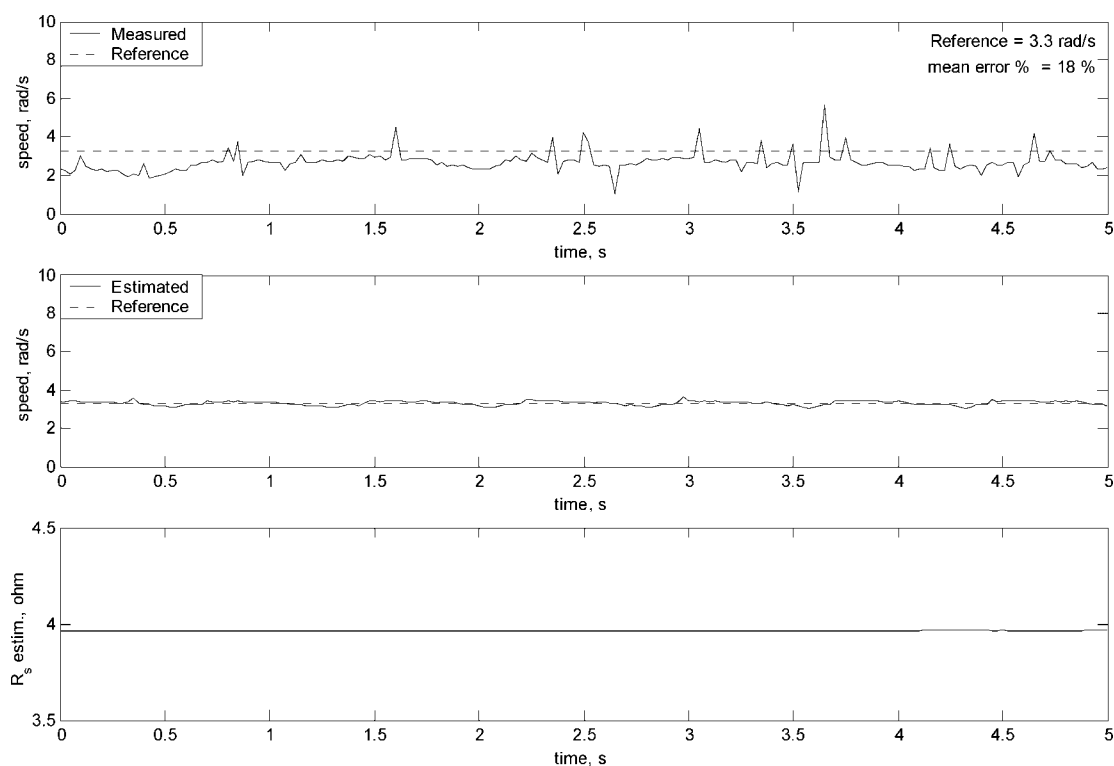


Fig. 14 Reference, estimated and measured speed and estimated R_s during a constant speed reference of 3.3 rad/s at no load (experimental)

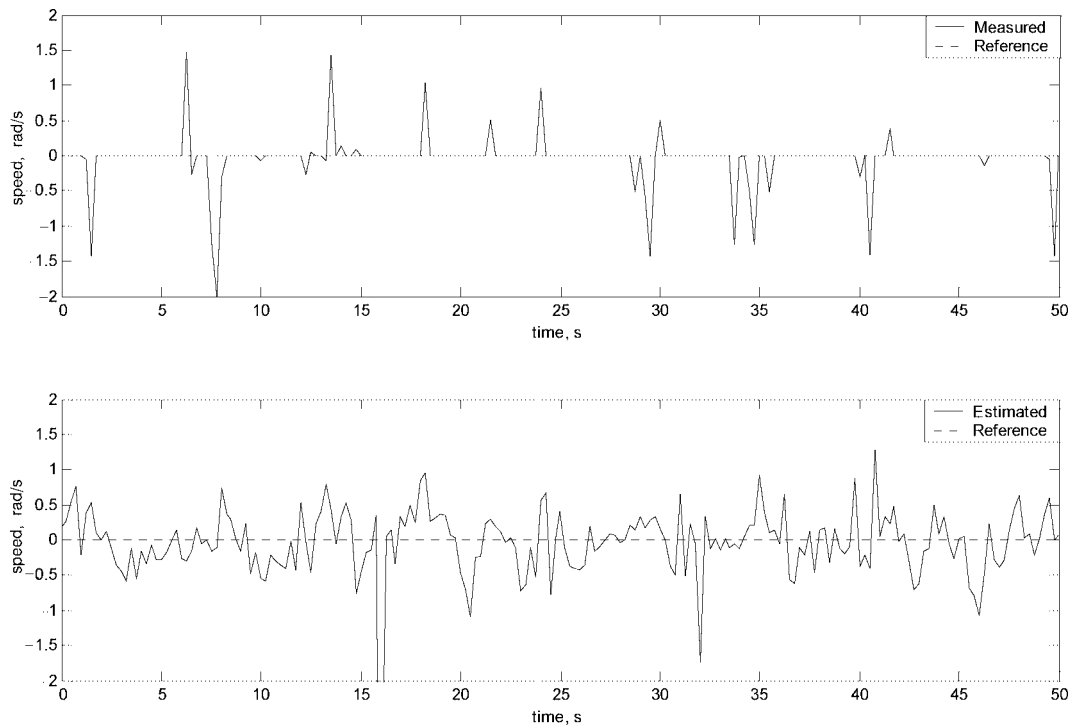


Fig. 15 Reference, estimated and measured speed at zero speed at no load (experimental)

7 CONCLUSIONS

This paper proposes a new sensorless technique for induction motor drives based on a hybrid MRAS-neural technique. This MRAS method is an improvement of an already developed neural MRAS based sensorless method in three aspects:

1. A more accurate discrete current model is used, based on the modified Euler integration, with resulting more integration accuracy and more stability at higher speeds.
2. An enhanced adaptive integration technique has been used in the reference model with a speed-varying filter transfer function with resulting higher accuracy in the open-loop flux integration than the fixed pole filter transfer function.
3. A completely new neural technique, the MCA EXIN + neuron, has been adopted to estimate the rotor speed; its scheduling makes it more powerful than the other existing techniques in terms of smoother transient, shorter settling time and better accuracy.

A theoretical analysis of the stability issues of the proposed observer in field weakening region has been done, showing a higher speed stability limit achievable with the Modified Euler integration method.

The MCA EXIN + MRAS observer has been experimentally tested on rotor flux oriented vector

control drive with induction motor and the results have proved its goodness in speed transients at low and high speed, at very low speeds (below 4 rad/s) and in zero-speed operation.

LIST OF SYMBOLS

- \mathbf{u}_s – space vector of the stator voltages in the stator reference frame
- u_{sD}, u_{sQ} – direct and quadrature components of the stator voltages in the stator reference frame
- \mathbf{i}_s – space vector of the stator currents in the stator reference frame
- i_{sD}, i_{sQ} – direct and quadrature components of the stator currents in the stator reference frame
- i_{sx}, i_{sy} – direct and quadrature components of the stator currents in the rotor-flux oriented reference frame
- $\boldsymbol{\psi}'_r$ – space vector of the rotor flux-linkages in the stator reference frame
- ψ_{rd}, ψ_{rq} – direct and quadrature component of the rotor flux linkage in the stator reference frame
- L_m – total static magnetising inductance
- R_s – resistance of a stator phase winding
- R_r – resistance of a rotor phase winding
- T_r – rotor time constant
- σ – total leakage factor

- p – number of pole pairs
 ω_r – angular rotor speed (in electrical angles per second)
 T_s – sampling time of the control system.

APPENDIX: TEST SETUP

The employed test set up consists of [17]:

- A three-phase induction motor with parameters shown in Table 1;
- A frequency converter which consists of a 3-phase diode rectifier and a 7.5 kVA, three-phase VSI;
- A DC machine for loading the induction machine with parameters shown in Table 2;
- An electronic AC-DC converter (three-phase diode rectifier and a full-bridge DC-DC converter) for supplying the DC machine of rated power 4 kVA;
- A dSPACE card (DS1103) with a PowerPC 604e at 400 MHz and a floating-point DSP TMS320F240;

Table 1 Parameters of the induction motor

Rated power P_{rated} , kW	2.2
Rated voltage U_{rated} , V	220
Rated frequency f_{rated} , Hz	50
Rated Speed, rad/s	149.75
Pole-pairs	2
Stator resistance R_s , Ω	3.88
Stator inductance L_s , mH	252
Rotor resistance R_r , Ω	1.87
Rotor inductance L_r , mH	252
3-phase magnetizing inductance L_m , mH	236
Moment of inertia J , $\text{kg} \cdot \text{m}^2$	0.0266

Table 2 Parameters of the DC machine

Rated power P_{rated} , kW	1.5
Rated voltage U_{rated} , V	300
Rated current I_{rat} , A	5
Rated speed, rad/s	150
Rated excitation voltage u_{extrat} , V	300
Rated excitation current i_{extrat} , A	0.33

REFERENCES

- [1] P. Vas, **Sensorless Vector and Direct Torque Control**. Oxford Science Publication, 1998.
- [2] K. Rajashekara, A. Kawamura, K. Matsuse, **Sensorless Control of AC Motor Drives**. IEEE Press, 1996.
- [3] H. Kubota, K. Matsuse, T. Nakano, **DSP-Based Speed Adaptive Flux Observer of Induction Motor**. IEEE Transactions on Industry Applications, Vol. 29, n° 2, pp. 344–348, March/April 1993.
- [4] Holtz, **Sensorless Control of Induction Motor Drives**. Proceedings of the IEEE, Volume: 90, n° 8, pp. 1359–1394, Aug. 2002.
- [5] R. D. Lorenz, T. A. Lipo, D. W. Novotny, **Motion Control with Induction Motors**. Proceedings of the IEEE, vol. 82, n. 8, August 1994.
- [6] P. L. Jansen, R. D. Lorenz, **Transducerless Position and Velocity Estimation in Induction and Salient AC Machines**. IEEE Transactions on Industry Applications, vol. 31, n. 2, March/April 1995;
- [7] P. L. Jansen, R. D. Lorenz, **Transducerless Field Orientation Concepts Employing Saturation-Induced Saliencies in Induction Machines**. IEEE Transactions on Industry Applications, vol. 32, n. 6, November/December 1996.
- [8] F. Briz, M. W. Degner, A. Diez, R. D. Lorenz, **Static and Dynamic Behavior of Saturation-Induced Saliencies and Their Effect on Carrier – Signal-Based Sensorless AC Drives**. IEEE Transactions on Industry Applications, vol. 38, n. 3, May/June 2002.
- [9] J. Holtz, Hangwen Pan, **Elimination of Saturation Effects in Sensorless Position-controlled Induction Motors**. IEEE Transactions on Industry Applications, Vol. 40, n° 2, pp. 623–631, March-April 2004.
- [10] A. Consoli, G. Scarcella, A. Testa, **Speed- and Current-sensorless Field-oriented Induction Motor Drive Operating at Low Stator Frequencies**. IEEE Transactions on Industry Applications, Vol. 40, n. 1, pp. 186–193, Jan.-Feb. 2004.
- [11] C. Shauder, **Adaptive Speed Identification for Vector Control of Induction Motors without Rotational Transducers**. IEEE Transactions on Industry Application, vol. 28, n° 5, pp. 1054–1061, September/October 1992.
- [12] H. Tajima, Y. Hori, **Speed Sensorless Field-Oriented of the Induction Machine**. IEEE Transactions on Industry Application, vol. 29, n° 1, pp. 175–180, January/February 1993.
- [13] L. Ben-Brahim, R. Kurosawa, **Identification of Induction Motor Speed using Neural Networks**. IEEE PCC, Yokohama, pp. 689–694, 1993.
- [14] M. Elloumi, L. Ben-Brahim, M. Al-Hamadi, **Survey of Speed Sensorless Controls for IM drives**. IEEE IECON 98, Vol. 2, pp. 1018–1023.
- [15] L. Ben-Brahim, S. Tadakuma, A. Akdag, **Speed Control of Induction Motor without Rotational Transducers**. IEEE Transactions on Industry Application, Vol. 35, n° 4, pp. 844–850, July/August 1999.
- [16] M. Cirrincione, M. Pucci, **An MRAS Based Speed Estimation Method with a Linear Neuron for High Performance Induction Motor Drives and Its Experimentation**. IEEE IEMDC 03, 1–4 June 2003, Madison, Wisconsin, USA.
- [17] M. Cirrincione, M. Pucci, G. Cirrincione, G. A. Capolino, **A New TLS Based MRAS Speed Estimation with Adaptive Integration for High Performance Induction Motor Drives**. IEEE Transactions on Industry Applications, June/July 2004.
- [18] M. Cirrincione, M. Pucci, G. Cirrincione, G. A. Capolino, **An Adaptive Speed Observer Based on a New Total Least-squares Neuron for Induction Machine Drives**. Conference Record of the IEEE Industry Applications Conference, 2004, vol. 2, 3–7 Oct. 2004, pp. 1350–1361.
- [19] M. Cirrincione, M. Pucci, **An MRAS Speed Sensorless High Performance Induction Motor Drive with a Predictive Adaptive Model**. On printing on IEEE Transactions on Industrial Electronics, April 2005.
- [20] M. Cirrincione, M. Pucci, **Sensorless Direct Torque Control of an Induction Motor by a TLS based MRAS Observer with Adaptive Integration**. Automatica, Regular Paper, n. 41, Novembre 2005, pp. 1843–1854.

- [21] M. Cirrincione, M. Pucci, G. Cirrincione, G. A. Capolino, **A New Adaptive Integration Methodology for Estimating Flux in Induction Machine Drives**. IEEE Transactions on Power Electronics, Vol. 19, n. 1, pp. 25–34, January 2004;
- [22] J. H. Matheus, K. D. Fink, **Numerical Methods Using Matlab**. 4th edition, 2004, Prentice-Hall Pub. Inc.
- [23] G. Cirrincione, M. Cirrincione, S. Van Huffel, **The GeTLS EXIN Neuron for Linear Regression**. IJCNN, Como (Italy), July 2000.
- [24] G. Cirrincione, **A Neural Approach to the Structure from Motion Problem**. Ph.D. thesis, INPG (Institut National Polytechnique de Grenoble) France, 1998.
- [25] J. Hu, B. Wu, **New Integration Algorithms for Estimating Motor Flux over a Wide Speed Range**. IEEE Transactions on Power Electronics, Vol. 13, n° 5, pp. 969–977, September 1998.
- [26] L. E. Borges de Silva, B. K. Bose, J. O. P. Pinto, **Recurrent-Neural-Network-Based Implementation of a Programmable Cascaded Low-Pass Filter Used in Stator Flux Synthesis of Vector-Controlled Induction Motor Drive**. IEEE Transactions on Industrial Electronics, Vol. 46, n° 3, pp. 662–665, June 1999.
- [27] J. O. P. Pinto, B. K. Bose, L. E. Borges de Silva, **A Stator-Flux-Oriented Vector-Controlled Induction Motor Drive with Space-Vector PWM and Flux-Vector Synthesis by Neural Network**. IEEE Transactions Industry Applications, Vol. 37, n° 5, pp. 1308–1318, September/October 2001.
- [28] J. Holtz, Q. Juntao, **Drift- and Parameter-Compensated Flux Estimator for Persistent Zero-Stator-Frequency Operation of Sensorless-Controlled Induction Motors**. IEEE Transactions on Industry Applications, Vol. 39, n° 4, pp. 1052–1060, July-Aug. 2003.
- [29] J. Holtz, Q. Juntao, **Sensorless Vector Control of Induction Motors at Very Low Speed Using a Nonlinear Inverter Model and Parameter Identification**. IEEE Transactions on Industry Applications, Vol. 38, n° 4, pp. 1087–1095, July-Aug. 2002.
- [30] M. Cirrincione, M. Pucci, G. Cirrincione, G. A. Capolino, **A New Experimental Application of Least-Squares Techniques for the Estimation of the Induction Motor Parameters**. IEEE Transactions on Industry Applications Vol. 39, n° 5, September/October 2003.
- [31] M. Cirrincione, M. Pucci, G. Cirrincione, G. Capolino, **Constrained Minimization for Parameter Estimation of Induction Motors in Saturated and Unsaturated Conditions**. IEEE Transactions on Industrial Electronics, vol. 52, n. 5, October 2005.

Jedan novi postupak estimacije brzine vrtnje vektorski upravljano asinkronog motora zasnovan na adaptivnom sustavu s referentnim modelom i neuronskim mrežama. U članku se predlaže novi postupak estimacije brzine vrtnje elektromotornog pogona s vektorski upravljanim asinkronim motorom. Postupak se zasniva na hibridnom adaptivnom sustavu s referentnim modelom (MRAS) i neuronskim mrežama. Takav postupak poboljšava prethodno razvijeni estimacijski postupak također zasnovan na »neuronskom MRAS-u«. U radu je realizirana integracija u otvorenoj petlji u referentnom modelu pomoću adaptivnog neuronskog integratora unaprijedenog s filtrom čija prijenosna funkcija ovisi o brzini motora. Adaptivni je model zasnovan na točnijem diskretnom strujnom modelu motora dobivenom modificiranom Eulerovom integracijom, što rezultira stabilnijim vladanju pogona u režimu slabljenja polja. Adaptivni je model nadalje on-line obučavan korištenjem poopćene metode najmanjih kvadrata (»MCA EXIN+neuron« postupak) pri čemu se koristi parametrirani algoritam učenja. Zbog boljeg ponašanja neurona u dinamičkim stanjima poboljšava se konvergencija estimacije brzine s većom točnošću i manjim vremenom smirivanja. Za eksperimentalnu provjeru predložene metode izgrađena je laboratorijska maketa. Dobiveni rezultati potvrđuju valjanost metode na veoma niskim brzinama (ispod 4 rad/s) i u režimu nulte brzine.

Ključne riječi: elektromotorni pogoni s asinkronim motorom, bessenzorsko upravljanje, adaptivno upravljanje s referentnim modelom, neuronske mreže

AUTHORS' ADDRESSES

Maurizio Cirrincione¹, Member IEEE
 Université de Technologie de Belfort-Montbéliard (UTBM),
 Rue Thierry Mieg, 90010 Belfort Cedex, France,
 m.cirrincione@ieee.org

Marcello Pucci, Member IEEE
 I.S.S.I.A.-C.N.R. Section of Palermo
 (Institute on Intelligent Systems for the Automation)
 Viale delle Scienze snc,
 90128 Palermo – Italy
 marcello.pucci@ieee.org

Giansalvo Cirrincione², Member IEEE
 Gérard-André Capolino, Fellow IEEE
 Department of Electrical Engineering
 University of Picardie-Jules Verne
 33, rue Saint Leu
 80039 Amiens – France
 g.cirrincione@ieee.org, Gerard.Capolino@ieee.org

Received: 2005-12-01

¹) Maurizio Cirrincione is now with the Université de Technologie de Belfort-Montbéliard (UTBM), Rue Thierry Mieg, 90010 Belfort Cedex, France and was with the ISSIA-CNR, Section of Palermo, viale delle scienze snc, 9128, Palermo, Italy.

²) Giansalvo Cirrincione is with the Department of Electrical Engineering University of Picardie-Jules Verne and funded

with a grant of ISSIA-CNR, Italy in the framework of the project *Automazione della gestione intelligente della generazione distribuita di energia elettrica da fonti rinnovabili e non inquinanti e della domanda di energia elettrica, anche con riferimento alle compatibilità interne e ambientali, all'affidabilità e alla sicurezza*. This work has been funded by the above project.